CHAPTER 7

THE EFFECT OF VOLUME SHAPE FACTOR ON THE CRYSTAL SIZE DISTRIBUTION OF FRAGMENTS DUE TO ATTRITION

7.1 Introduction

In a crystallizer, particles are kept in suspension by means of a pump or a stirrer. This results in attrition of crystals owing to contact with either the high-speed impeller of the pump or the stirrer. Attrition occurs also as the result of collisions of crystals with each other and with the wall. When the impact energy exceeds the crystal strength, the consequence is the fracture of the crystals. Thus the crystal geometry changes substantially and it seldom grows to its geometric shape. ANG and MULLIN (1979) measured the volume shape factor of nickel ammonium sulphate crystals and found a value of 0.58 ± 0.02. In an industrial crystallizer a wide variation in shape factor may be expected.

In the present work, the steady state CSD of fragments with volume shape factor dispersion generated by the attrition mechanism is predicted by incorporating

the MC technique into the physical model developed by GAHN and MERSMANN (1997). In their work the rate of generation of attrition fragments is assumed to be contributed by the high energies impact of crystals with the impeller. This impact may occur with crystal faces, edges and corners. Because of the fluctuating turbulence in the liquid phase, the particles are almost randomly oriented in the vicinity of the impeller. The contacts with corners are therefore most likely to result in high local stress due to the small area of contact. Hence repeated contacts would result in rounded-off crystals of reduced size, provided that there is no competing mechanism of crystal growth.

The shape factor of the crystals may vary widely depending on the attrition process and the nature of the substance. GAHN and MERSMANN (1997) have assumed cubic configuration for all crystals before and after the fracture. The present simulation scheme is free from such restriction and can accommodate practically all types of shape factor distribution. In this work, a normal distribution has been assumed with $\alpha = 1$ and $\alpha = 0.5236$ as the two limits, which conform to cubic and spherical configurations respectively.

MC technique (SEN GUPTA and DUTTA, 1990a/91) has been used to generate random samples of volume shape factor and to simulate the corresponding CSD under the shape factor dispersion effect.

7.2 Physical attrition model

The physical model (GAHN and MERSMANN, 1997) employed here is based on the following assumptions:

(i) Only the contact of a crystal corner with another flat and much harder object (steel impeller) is considered.

(ii) The crystal faces forming that corner are replaced by a cone having an included angle of 120° (Figure 7.1).

(iii) The impact energy causes a force acting normally on the corner (no sliding contact and no rotation of the crystal).

(iv) Fracture is assumed to initiate after complete loading. The formation and propagation of cracks occur instantaneously and are determined by this quasi-static stress field (the effect of elastic waves is assumed to be negligible).

(v) The mechanical properties of the crystalline substance can be replaced by average isotropic values (Poisson's ratio, $\nu = 0.25$), which are assumed to be independent of the strain rate.

(vi) The newly created surface caused by the formation of a fragment is proportional to the elastic strain energy stored in the volume of this fragment (Rittinger's law).

(vii) Since the required pressure for plastic deformation is high, it is assumed here that ductility is restricted to a region limited by the area of contact, and that the material is elastic elsewhere.

(viii) Because of plastic flow in the contact region, it is assumed that fracture only takes place in the elastic stress field.

(ix) The volume where plastic deformation occurs is generally small compared to the volume, which is removed from a crystal by impact. At a distance 'r' from the original corner of the cone, the elastic field can be considered to be created by a point force acting at the corner of the cone (Figure 7.1b).

(x) Average strain energy density is constant at a given distance r and is not a function of the polar coordinates θ and ϕ (Figure 7.1b).

(xi) After complete loading, the impact energy is equivalent to the energy necessary for the plastic deformation of the corner and the total elastic strain energy stored in the cone.

(xii) The characteristic size 'a' is only determined by the hardness of the crystal and not by the ratio of hardness to shear modulus.

With the above assumptions, the equation relating the fragment size (L) with the mechanical properties and the distance from the peak of the cone (r) is given by:

$$L \approx \frac{3\mu\Gamma}{W_p^{4/3} H^{2/3} K_r} r^4 \tag{7.1}$$

where the characteristic size of a fragment produced at a distance r is proportional to r^4. By combining Eq. (7.1) with

$$\frac{dV_{el}}{dL} = \alpha N L^3 q_o(L) \tag{7.2}$$

and

$$\frac{dV_{el}}{dr} = \pi r^2 \tag{7.3}$$

the following equation is obtained:

$$\alpha N q_o(L) \approx \frac{\pi}{9} \frac{W_p H^{1/2} K_r^{3/4}}{(\mu\Gamma)^{3/4}} L^{-3.25} \tag{7.4}$$

The number density function is defined as

$$\int_{L_{min}}^{L_{max}} q_o(L)dL = 1 \tag{7.5}$$

where

$$q_o(L) = \frac{2.25}{L_{min}^{-2.25} - L_{max}^{-2.25}} L^{-3.25} \tag{7.6}$$

and for the total number of fragments

$$N \approx \frac{\pi}{21} \frac{W_p H^{1/2} K_r^{3/4}}{\alpha(\mu\Gamma)^{3/4}} \left(\frac{1}{L_{min}^{2.25}} - \frac{1}{L_{max}^{2.25}} \right) \tag{7.7}$$

Eq. (7.1) indicates that the small fragments will be produced in the vicinity of the contact zone 'a' or in the region of the plastic-elastic boundary ($a^4/r^4 = 1$) where the strain energy density is the highest. Therefore, the minimum size of the fragment is given by

$$L_{min} \approx \frac{32}{3} \frac{\mu\Gamma}{K_r H^2} \tag{7.8}$$

A combination of Eqs. (7.7) and (7.8) gives the approximate solution for the number of fragments produced.

$$N \approx 7 \times 10^{-4} \frac{W_p H^5 K_r^3}{\alpha \mu^3 \Gamma^3} \tag{7.9}$$

The maximum size of the fragments can be calculated to be about

$$L_{max} \approx r_{max}/2 \tag{7.10}$$

and the total volume removed from the attrition process is

$$V_a \approx \frac{2}{3} \frac{H^{2/3} K_r}{\mu \Gamma} W_p^{4/3} \tag{7.11}$$

By combining Eq. (7.9) and (7.11),

$$V_a \approx k^1 (\alpha N)^{4/3} \tag{7.12}$$

The set of equations presented here can only be used when the relevant material properties are known, i.e. elastic constants, hardness and fracture resistance.

An isotropic material has two independent elastic constants i.e., the shear modulus μ, and Poisson's ratio ν, from which all the other possible constants can be determined. Assuming that impacts on a crystal are distributed statistically in all axis directions, the effective (isotropic) elastic properties can be estimated from these constants. In the above relations, the shear modulus was used and the quasi-isotropic shear moduli μ_{VRH} of the substances under consideration are given in Table 7.1.

The hardness of a solid is usually considered to be its resistance to local plastic deformation. By assuming that the contact pressure of a plastically deformed cone and the Vickers hardness H_v are the same, we can use the appropriate Vickers hardness (Table 7.1) of a substance in the above equations.

The fracture resistance is given in the form (Γ/K_r). This ratio can be estimated by performing indentation tests using the Vickers indenter. Since at an applied critical load, cracks will form around the indentation when the substance exhibits brittleness. The critical work can be related to the material properties according to

$$\frac{\Gamma}{K_r} = \frac{\kappa}{5.2}\frac{W_c^{1/3}H^{5/3}}{\mu} \tag{7.13}$$

where the parameter κ accounts for the stress field. It was observed that the stress fields created by the Vickers indentation and crystals-impeller impacts were similar

but not equal. GAHN and MERSMANN (1997) concluded that $\kappa = 0.5$ would provide the best fit between the theoretical and experimental results. The critical work values for the substances under studied are listed in Table 7.1.

The incorporation of the MC technique to study the effect of volume shape factor in the physical model of GAHN and MERSMANN (1997) is outlined in the following section.

7.3 The simulation scheme

It is evident from Eq. (7.6), that the number density function is proportional to the fragment size as follows:

$$q_o \propto L^{-3.25} \tag{7.14}$$

Since the fragment size is proportional to r^4 (Eq. 7.1), therefore

$$q_o \propto r^{-13} \tag{7.15}$$

By plotting $\log q_o$ against $\log r$, a straight line with slope of -13 is obtained. The total number of crystal produced is essentially determined by the lower limit of

the size distribution, whereas the upper limit has practically no influence. We could randomize Eq. (7.15) by considering

$$\log RND = -13\log r + c \tag{7.16}$$

with the boundary condition of $RND = 1$ with $r = a$,

$$c = 13\log a \tag{7.17}$$

therefore,

$$r = \exp\left(\frac{13\log a - \log RND}{13}\right) \tag{7.18}$$

By combining Eqs. (7.18), (7.9) and (7.1), the fragment sizes for N number of crystals generated from the attrition of one crystal can be determined. The volume shape factor in Eq. (7.9) is assumed to be normally distributed according to

$$\alpha = \frac{\alpha_{max} + \alpha_{min}}{2} \pm \sqrt{-2\left(\frac{\alpha_{max} - \alpha_{min}}{6}\right)^6 \log RND} \tag{7.19}$$

The detailed procedure of generating random samples of volume shape factor from the normal density function is given in Appendix I.3. The simulation process is outlined in Appendix VII.1.

7.4 Results and discussion

In this work the simulation was carried out for the magnesium sulphate heptahydrate (MS) and potash alum (PA) crystals to compare results with those reported by GAHN and MERSMANN (1997). The relevant material properties, as tabulated by by GAHN and MERSMANN (1997), for MS and PA are listed in Table 7.1. The simulation was carried out for three different impact energies, e.g. 1E-4, 1E-5 and 1E-6 J. GAHN and MERSMANN (1997) took 50 sample crystals for each experiment on attrition. In this work the same sample size was used for simulation purposes. The sample programs and simulated results for an impact energy of 1E-5J and $\alpha = \alpha_n$ are outlined in Appendix VII.2 for MS and PA.

For MS, Table 7.2 provides a comparison of the CSD of fragments generated with an impact energy of 1E-4J for $\alpha = \alpha_n$ with two discrete shape factors, namely, $\alpha = 0.5236$ and $\alpha = 1$. The number distribution of fragments for these substances are tabulated at different intervals between L_{min} and L_{max}. The value of L_{min} is obtained from Eq. (7.8) while L_{max} from combining Eq. (7.1) and (7.10). By assuming $\alpha = \alpha_n$, the number of fragments generated is higher than the hypothetical

number of cubic crystals but is lower than the number of spherical crystals. The number of fragments for three different cases is given in Table 7.2. It is observed that the differences are more prevalent in the smaller fragment sizes. In short the CSD of fragments for normally distributed volume shape factor lies between two extreme cases of cube and spherical geometry.

The total volume removed by attrition for each sample, as obtained from Eq. (7.12), is indicated in the Table 7.2. The value of V_a was found to be the same for the three volume shape factor parameters. Any variation in the volume shape factor is compensated by the total number of fragments. The value of V_a is within the range of the data reported by GAHN and MERSMANN (1997).

Table 7.3 lists the CSD of fragments for PA with an impact energy of 1E-4J for three different values of α. The simulation results for PA generated a significantly higher amount of fragments as compared to MS. As the critical work (W_c) required to form crack in PA is lower than that of MS, it implies a lower fracture resistance and higher hardness (also increase in brittleness). Thus the energy necessary to form attrition also decreases. Therefore, the same amount of energy would produce a greater number of fragments for PA with a higher number of small fragments. This also explains the reason for a higher V_a for PA as compared to MS. In addition, substance like PA with a low fracture resistance and higher hardness as compared to MS has also resulted in a wider CSD of fragments.

The results in Table 7.2 and 7.3 are plotted in log N vs. Log L as shown in Figure 7.2 and 7.3 respectively. A least-square method was used to find the slopes of the three lines and the values are indicated in these figures. The slopes are found to deviate slightly from the expected average value of -3.25 (Eg. 7.6) as in GAHN and MERSMANN physical model. Furthermore, the slopes are found to be insensitive to the volume shape factor variation.

The fragment CSDs of MS and PA for the three volume shape factors with an impact energy of 1E-5J are plotted in Figure 7.4 and 7.5 while those for 1E-6J are plotted in Figure 7.6 and 7.7. For both the substances, the fragments are distributed over a narrower range of sizes for the impact energy of 1E-6J. At such low energy, the point force acting at the corner of the cone causes the stress to propagate nearer from the original peak of the cone resulting in a decrease in r_{max}. Since the size of a fragment is a function of r, smaller size fragments are obtained with lower energies.

The total numbers of fragments are also indicated in Figures 7.3 through 7.7. It was found to be lower for the lower impact energy. For the case of MS with $\alpha = \alpha_n$, an impact energy of 1E-4 J generated 1,080,871 fragments while 1E-5 and 1E-6 generated 109,814 and 11,096 fragments respectively. It is obvious from Eq. (7.7) that the total number of fragments produced is directly proportional to the impact energy. An increase in this energy by a factor of ten resulted in an increase in the number of fragments by the same factor.

The slopes of the lines are as shown in Figures 7.3 through 7.7. All the slopes are between -3.25 to -3.58. The deviations from the expected average slope of -3.25 are found to be insignificant.

7.5 Conclusions

Monte Carlo technique is a versatile and powerful tool for simulating the CSD of fragments as a result of the attrition process. The basic advantage of MC is that one could obtain the CSD under all possible dispersion effects. In the present contribution, a normal distribution has been used to represent dispersion in volume shape factor from a physical standpoint for generating the fragment size distribution in GAHN and MERSMANN's model. The number density of the fragments was plotted as a function of particle size in a logarithmic plot. The CSD of fragments with normally distributed shape factor are found to lie between two extreme cases of cubic and spherical geometry. The result obtained is consistent with the physical model with the slopes of the fragment distribution plots in good agreement with the expected average values of -3.25.

In addition to the three measurable mechanical properties, e.g. hardness, fracture resistance and a quasi-isotropic constant, only one additional parameter is required to simulate the CSD using the MC technique, i.e. the impact energy. The

CSD of fragments are distributed with a wide range at higher impact energy and the total number of fragments is directly proportional to the impact energy.

Table 7.1 Vicker Hardness H_v, average shear modulus μ_{VRH}, and the critical work to form cracks W_c, for magnesium sulphate heptahydrate and potash alum

Substance	H_v (10^6 Pa)	μ_{VRH} (10^9 Pa)	W_c (10^{-10} J)
Magnesium sulphate (MS) heptahydrate	649	9.06	48
Potash alum (PA)	754	7.96	7

Table 7.2 The fragments size distribution for magnesium sulphate heptahydrate (MS) with $\alpha = 0.5236$, $\alpha = \alpha_n$ and $\alpha = 1$ at W_p = 1E-4 J

Fragment size (μm)	No. of fragment [+]		
	$\alpha = 0.5236$	$\alpha = \alpha_n$	$\alpha = 1$
1	1148321	793428	600101
3	338718	233018	178025
5	71074	48715	37592
10	6148	4235	3260
15	1349	893	750
20	410	313	221
25	194	128	121
30	137	88	83
40	67	44	28
60	32	9	19
Total	1566450	1080871	820200

$L_{min} = 2$ μm

$L_{max} = 97$ μm

$V_a = 2.93957 \times 10^{-11}$ m^3

Table 7.3 The fragments size distribution for potash alum (PA) with $\alpha = 0.5236$, $\alpha = \alpha_n$ and $\alpha = 1$ at W_p = 1E-4 J

Fragment size (μm)	No. of fragment [+]		
	$\alpha = 0.5236$	$\alpha = \alpha_n$	$\alpha = 1$
1	10438645	7413789	5465729
3	245377	173892	128460
5	51606	36514	26961
10	4367	3163	2286
15	994	721	522
20	293	230	191
25	151	109	66
30	100	69	55
40	49	32	24
60	14	9	3
80	4	2	3
Total	10741600	7628530	5624300

L_{min} = 1 μm

L_{max} = 115 μm

$V_a = 4.80697 \times 10^{-11}$ m^3

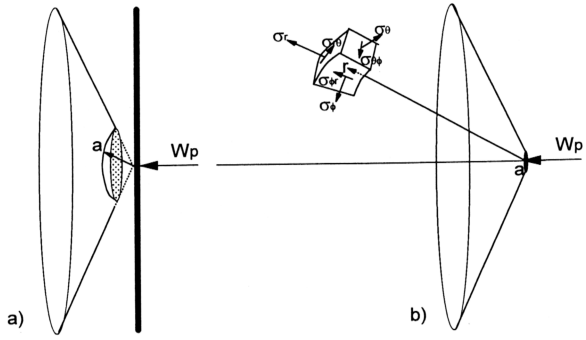

ure 7.1 (a) Assumed geometry of the plastically deformed zone
(b) Stress created in the elastic zone

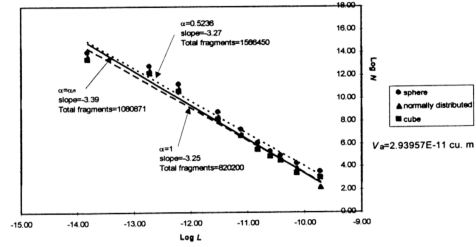

Figure 7.2 Particle size distribution of fragments for MS at W_P=1E-4J with α=0.5236, $\alpha=\alpha_n$ and α=1

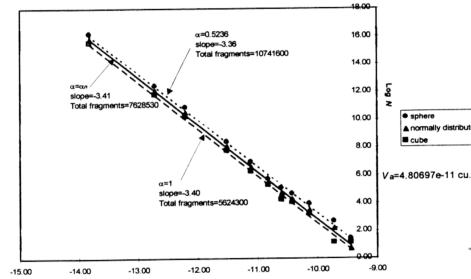

Figure 7.3 Particle size distribution of fragments for PA at W_P=1E-4J with α=0.5236, $\alpha=\alpha_n$ and α=1

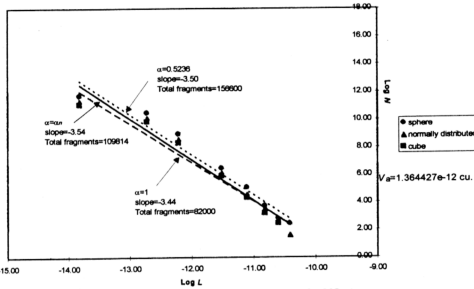

Figure 7.4 Particle number distribution of fragments for MS at W_P=1E-5J with α=0.5236, $\alpha=\alpha_n$ and α=1

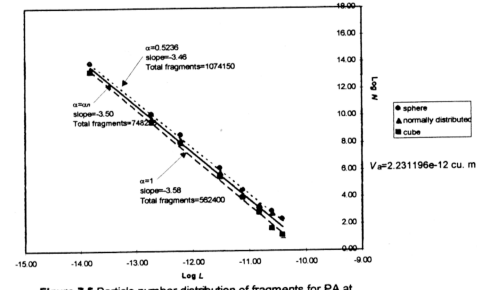

Figure 7.5 Particle number distribution of fragments for PA at W_P=1E-5J with α=0.5236, $\alpha=\alpha_n$ and α=1

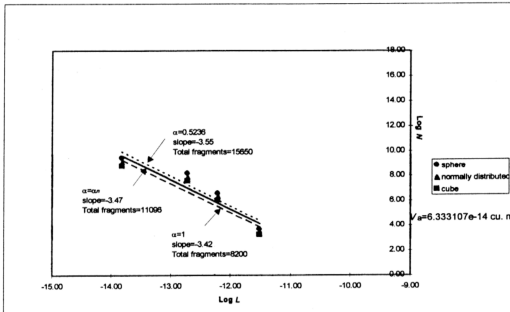

Figure 7.6 Particle number distribution of fragments for MS at Wp=1E-6J with α=0.5236, α=α_n and α=1

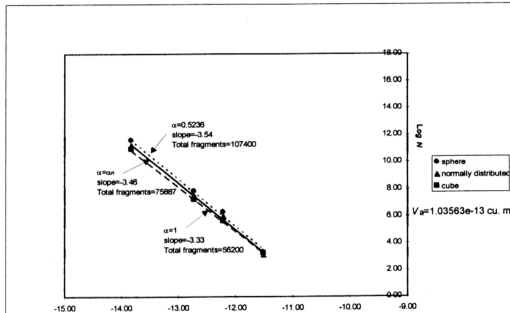

Figure 7.7 Particle number distribution of fragments for Pa at Wp=1E-6J with α=0.5236, α=α_n and α=1